

Applied TEM Approach for Micro/Nanostructural Characterization of Carbon Nanotube Reinforced Cementitious Composites

Nirupam Aich, Nima Zohhadi, Ifthekeer A. Khan, Fabio Matta, Paul Ziehl and Navid B. Saleh*

Department of Civil and Environmental Engineering, University of South Carolina, SC 29208, Columbia

Abstract: A novel colloidal technique for transmission electron microscopy (TEM) of graphitic nano-reinforced cementitious (GNRC) composites was developed. Single-walled and multiwalled nanotubes (SWNTs and MWNTs) were functionalized using an acid etching technique to obtain stable aqueous suspensions that were incorporated in the mix design of a cement paste. Effective functionalization was demonstrated by Raman spectroscopic measurements and time resolved dynamic light scattering measurements. The functionalized nano-reinforcement and binding characteristics were observed at the nanoscale for the first time using high resolution TEM imaging. Functionalized CNTs were found to be well distributed and preferentially associated with the cementitious matrix. This newly developed colloidal technique for TEM imaging of GNRC composites is a viable approach to characterize the interfacial compatibility between graphitic nano-reinforcement and cementitious matrices.

Keywords: Carbon nanotube, nano-reinforcement, cementitious materials, TEM, colloidal technique.

1. INTRODUCTION

Graphitic nano-reinforced cementitious (GNRC) composites show great promise as an improved class of structural material [1] with enhanced microcrack control capabilities resulting in better damage tolerance [2], fracture toughness [3], and improved flexural strength and stiffness [4-6]. In addition, the decrease in electrical resistivity compared to conventional cementitious composites [7] makes structural GNRC composites attractive as self-sensing and health monitoring materials [8]. The improved performance of these novel composites largely depends on the nanomaterial dispersion properties [4, 9-10] and chemical bonding characteristics within the cementitious matrix. Dispersion—of the highly aggregating carbonaceous nanofibers—in aqueous suspensions is achieved by evoking chemical functionality to the nano-reinforcement surfaces, typically accomplished through acid etching [6] or surfactant coating [11] procedures. The resulting functional groups act as chemical binding sites for the metal ions in the calcium oxide/silica/alumina matrix of cement, thus providing key compatibility attributes to the composite system [5]. Mechanistic understanding of material compatibility between graphitic nano-reinforcement and cementitious matrices requires development of novel characterization techniques to better probe the interface between the nano-reinforcement and the surrounding cementitious matrix.

Transmission electron microscopy (TEM) is one of the most effective characterization techniques for engineered nanomaterials. TEM can provide information on nanomaterial size, shape, and crystallographic structure along with particle distribution at the atomic scale [12-16]. In situ TEM can be performed for dynamic observation of the morphological and nanostructural changes due to reactions among nanomaterials and also due to mechanical stress applied *in situ* on a nanomaterial or nanocomposite [17-18]. Analytical TEM equipped with electron energy loss spectroscopy (EELS), energy dispersive spectroscopy (EDS), and dark field imaging can reveal chemical information on complex matrices [13, 19] and can serve in failure analysis of nano-electronics (e.g., semiconductors) [20]. TEM is also employed to study composite materials' morphology and dispersion characteristics [21], particularly of those that include nanomaterial in polymer matrices; e.g., polymer/clay composites [22], nanoparticle glass composites [23], nanotube-nylon 6 composites [24-25], thermoplastic elastomers with multi-walled carbon nanotubes [26], and nanotube/epoxy composites [27-29]. Innovative approaches in sample preparation—for example, ultrathin nanocomposite film preparation using microtome methods [27], and milling of the composites through Focused Ion Beam (FIB) techniques [30-32]—are being adopted to obtain high quality images.

Challenges still remain to perform TEM on cementitious composites due to the difficulties in processing material samples and forming ultrathin electron transparent sections that can be mounted on the TEM grid [33]. This has restricted electron imaging

*Address corresponding to this author at the Department of Civil and Environmental Engineering, University of South Carolina, SC 29208, Columbia; Tel: 803-777-2288; Fax: 803-777-0670; E-mail: salehn@enr.sc.edu

usage in cementitious composite characterization to scanning electron microscopy (SEM) [34-36]; a technique that can reveal key surface characteristics of composites but with a lesser degree of magnification and at a coarser scale [20, 37]. Developing novel approaches to image at the interfacial scale (with TEM) is highly desirable to facilitate the investigation of compatibility characteristics of graphitic nano-reinforcement and cementitious matrices.

This paper presents a novel colloidal technique to prepare GNRC composite samples for high resolution TEM imaging. Single- and multi-walled carbon nanotubes (SWNTs and MWNTs) were acid etched to obtain well dispersed suspensions in water. The carboxylated SWNTs and MWNTs were characterized using Raman spectroscopy to determine the extent of defects and dynamic light scattering was used to determine colloidal stability. Cementitious composite samples reinforced with carboxylated SWNTs and MWNTs were prepared per ASTM C305. Representative GNRC composite samples were collected by pulverizing the material at fracture surfaces and dispersing the powder in ethanol by sonication. TEM was performed using a high resolution transmission electron microscope (HRTEM) at an accelerating voltage of 300 kV. To the best of the authors' knowledge, this study is the first to propose such a colloidal approach to perform TEM imaging on GNRC composites, characterizing material compatibility at the matrix interfaces.

2. EXPERIMENTAL

2.1. Preparation and Characterization of Functionalized SWNTs and MWNTs

SWNTs and MWNTs were procured from commercial sources (Cheap Tubes Inc., Brattleboro, VT). The supplier claimed purity of SWNT and MWNT samples of 90% and 95% by mass with bulk densities of 0.14 and 0.27 g/cm³ at 20°C, respectively. The inner diameters of the tubes were specified as 0.8-1.6 nm and 2-5 nm with average tube lengths of 5-30 μm and 10-30 μm for SWNTs and MWNTs, respectively. Both carbon nanotubes (CNTs) were independently characterized for this study.

SWNTs and MWNTs were individually functionalized by etching the surfaces with strong oxidants as described elsewhere [38]. In short, for each CNT, 187.5 g of 98% ammonium persulfate (Sigma-Aldrich, St. Louis, MO), 13.6 mL of 95-98% sulfuric acid

(Acros, Thermo Fisher Scientific, NJ), and 236.4 mL of deionized (DI) water (Barnstead) were added to a 300 mL conical flask and stirred with a magnetic stirrer (VWR stirrer, Henry Troemner LLC., Thorofare, NJ) for 24-72 hours or until a clear solution was achieved. The solution was filtered through a 0.45 μm PVDF membrane filter (Millipore, Billerica, MA) to remove excess undissolved ammonium persulfate. A mass of 500 mg CNT (SWNTs or MWNTs) was added to the clear filtrate. The mixture was first sonicated for 10 minutes using an ultrasonic dismembrator S-4000 (Misonix, Inc., Farmingdale, NY) and later stirred at 1200 rpm for 24 hours. The suspension was then filtered through a PVDF filter under vacuum and washed with DI water until the filtrate reached a pH of nearly 7.0. Filtration was performed using a filter holder with fritted glass support (VWR International, West Chester, PA). The residue was stored in a dessicator cabinet (Fisher Scientific, Pittsburg, PA) for 72 hours and functionalized CNTs were obtained as dried flake/powder. After functionalization, 600 mg of CNTs (SWNTs or MWNTs) were introduced to 300 mL of DI water and sonicated for 10 minutes to prepare a 2 g/L aqueous suspension.

Cluster morphology and the extent of defects for pristine and functionalized SWNTs and MWNTs were primarily characterized with TEM and Raman spectroscopy, respectively. An H-9500 HRTEM (Hitachi High Technologies America, Inc, Pleasanton, CA) was used to image pristine and functionalized SWNTs and MWNTs, herein denoted as 'f-SWNTs' and 'f-MWNTs', respectively. TEM grids were prepared using a standard protocol for carbon nanotube characterization [39-41]. 0.5 mg of dry pristine or functionalized CNTs were sonicated in 10 mL of ethanol for 10 minutes using an ultrasonic bath sonicator (Branson, Danbury, CT) and a few drops were placed on a copper TEM grid coated with carbon film. The drops were allowed to dry on a hot plate for 5 min. Representative images for each sample were obtained using a randomized grid sampling technique [40-41] at varied magnification (10 k× to 100 k×) under an accelerating voltage of 300 kV.

Raman spectra for pristine and functionalized CNTs were recorded using a JY Horiba Labram Raman spectrometer (HORIBA Instruments Inc., Irvine, CA) equipped with a liquid-nitrogen-cooled charged coupled device (CCD) detector, and a HeNe (632.817 nm) laser for excitation [42]. Dry SWNT and MWNT powders were added to a pre-cleaned glass slide and the laser was focused on the sample surface. A representative spectrum was obtained as an average of five scans—

where each spectrum was collected over 120 s integration time. Details of the experimental protocol are presented elsewhere [40-41].

Colloidal stability of the aqueous suspensions of f-SWNTs and f-MWNTs was determined using time resolved dynamic light scattering (TRDLS). An ALV/CGS-3 compact goniometer system (ALV-Laser Vertriebsgesellschaft m.b.H., Langen/Hessen, Germany) equipped with 22 mW HeNe Laser at 632 nm wavelength (equivalent to 800 mW laser at 532 nm) and high QE APD detector with photomultipliers of 1:25 sensitivity was used to perform these measurements. The detailed TRDLS protocol is described in earlier studies [40-41]. In short, 2 mL of diluted nanotube suspension (concentration of each sample being ≤ 1 mg/L) was added to a rigorously cleaned borosilicate [40-41] glass vial and vortex mixed (using VWR Vortexer, Henry Troemner LLC., Thorofare, NJ) prior to initiating the TRDLS measurements. The laser was operated at full exposure level and scattering data was collected at a 90° scattering angle for 15 seconds to generate average hydrodynamic radius data points. A continuous measurement was performed for at least 30 minutes. The scattering data were used to generate profiles for f-SWNT and f-MWNT cluster size distribution with built-in 'cumulant algorithm' of the ALV software.

2.2. GNRC Specimen Preparation and Colloidal Technique for TEM Samples

GNRC composite specimens with $6.3 \times 6.3 \times 25.4$ mm dimensions were prepared per ASTM C305 by

mixing conventional Type III Portland cement with water using a water/cement (w/c) ratio of 0.485 (Figure 1). Either f-SWNTs or f-MWNTs were incorporated to the cement paste as 2 g/L aqueous suspension, which corresponds to 0.1% by weight of cement (wt%). The GNRC composite specimens were cast and moist cured for 24 hours and then demolded and air cured for 28 days. The GNRC composite strips were cracked by imparting a bending stress exceeding the modulus of rupture. The fracture surfaces were thus exposed from which GNRC composite material was removed. The powder for TEM analysis was obtained by placing this material between two plastic sheets and pulverizing with a pestle. This sample preparation process is illustrated (step by step) in Figure 2 for clarity.

A small amount (approximately 1-2 mg) of the GNRC composite powder containing either f-SWNTs or f-MWNTs was added to 5 mL ethanol to facilitate CNT exfoliation. A suspension was prepared by sonicating the mixture using an ultrasonic bath dismembrator (Bransonic, Danbury, CT). A few drops of the sonicated suspension were added to the copper TEM grids coated with carbon film. TEM was performed following the procedure described above to characterize pristine and functionalized CNTs.

3. RESULTS AND DISCUSSION

3.1. Characteristics of f-SWNTs and f-MWNTs and their Aqueous Dispersions

TEM micrographs presented in Figure 3a-d of pristine and functionalized SWNTs and MWNTs



Figure 1: GNRC composite strips (dimensions $6.3 \times 6.3 \times 25.4$ mm) for TEM characterization.

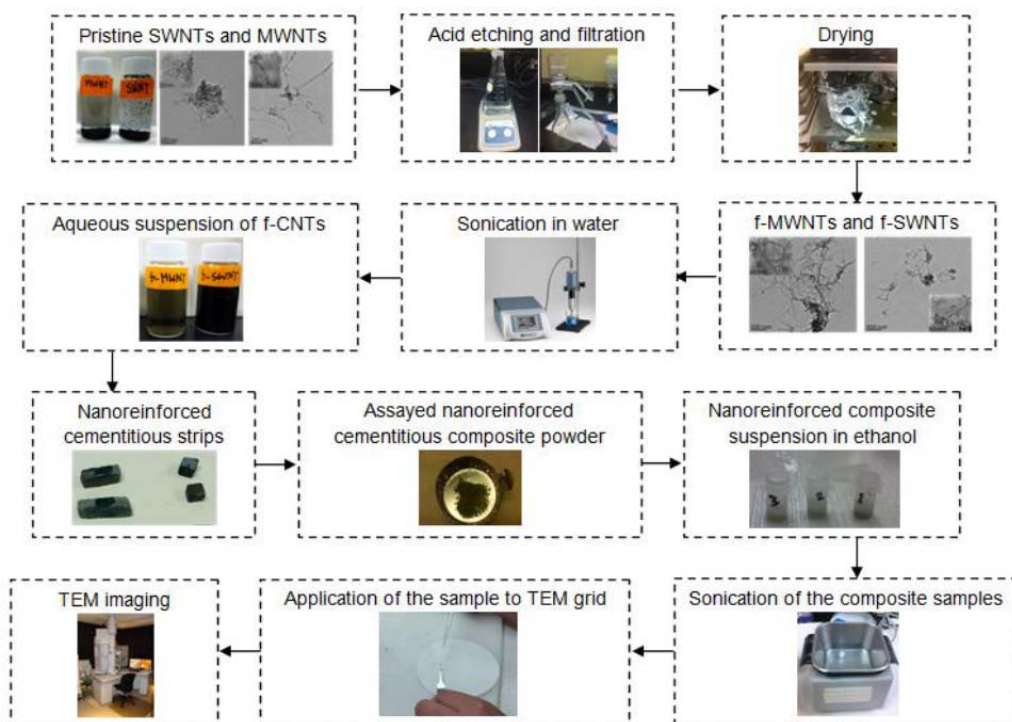


Figure 2: Schematic of TEM sample preparation steps involved in colloidal approach.

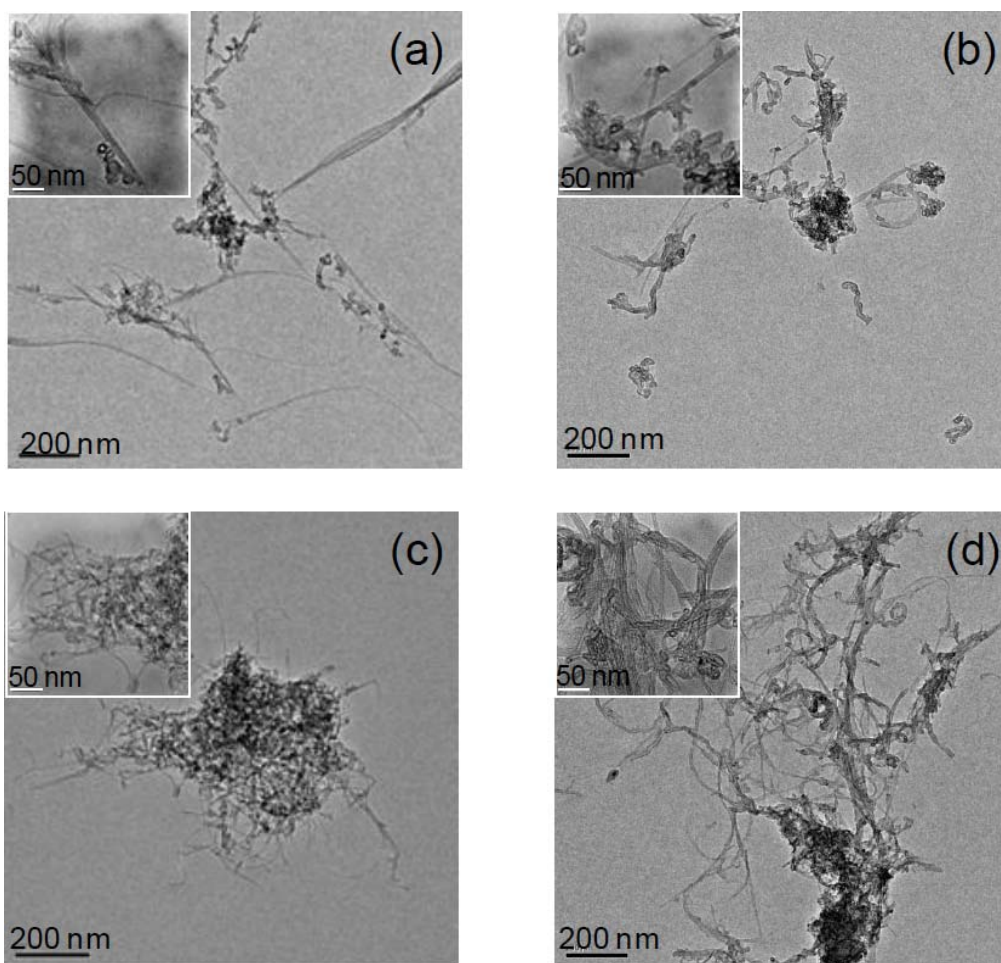


Figure 3: Representative TEM micrographs of SWNTs (a) pristine and (b) functionalized and MWNTs (c) pristine and (d) functionalized. Insets represent higher magnification images of SWNTs and MWNTs.

document effective functionalization of the CNTs. Figure 3a and 3c show highly bundled, aggregated, and relatively (in multi-micron scale) long pristine SWNTs and MWNTs, respectively. The insets of these images further illustrate the bundled state of the CNTs. Figure 3b and 3d show relatively debundled and declustered CNTs upon functionalization. Such debundling had plausibly occurred from the invoked electrostatic repulsion between tubes as a result of the oxidation process [43]. The higher magnification inset micrographs present evidence of shorter functionalized CNTs, which is consistent with previous findings reported in the literature [5-6]. These short tubes or fragments of tubes were likely generated through tube breakage during the acid etching process [44-45]. Such shortening and tube breakage, as observed here and in earlier literature, occurs due to C-C bond breakage and subsequent oxidation at these sites and at the existing defect sites on CNTs during sonication and use of strong oxidants, such as acids [44, 46-48]. Electron deficient carbon atoms at the defects and edge extremities attract electron excess molecules oxygen and typically form $-COOH$ groups at such sites [48-49]. Thus functionalization of SWNTs and MWNTs not only shorten the tubes but also debundle them due to the repulsive interaction emanating from added $-COOH$ groups. The effect of functionalization is further illustrated through defect and dispersion characterization as presented later in this section.

Raman spectra collected on pristine and functionalized SWNTs and MWNTs provide evidence of successful functionalization through defect characterization as presented in Figure 4a-b. Spectral results were analyzed for peaks near 1600 cm^{-1}

(denoted as the G-band holding graphitic signature) and near 1350 cm^{-1} (denoted as the D-band that represents defects in the CNT graphitic structure) [50] to obtain relative defect ratios—i.e., D/G ratio of integrated peaks. Defects, identified as lack in hexagonal structure of carbon atoms orientation as well as bond breakage, are present even in pristine nanotube surfaces; which occur during CNT synthesis in elevated temperature [51]. These defected sites give rise to Raman scattering at defect mode and can be quantified through this spectroscopic technique. Such defect formation is further pronounced upon functionalization with strong oxidants, which induces a stronger peaking at D-band region [51-53]. Quantitation of Raman response at this region allows to evaluate relative effectiveness of functionalization through the D/G ratio comparison, discussed earlier. The estimated D/G ratios presented in Figure 5 show an increase from 0.06 to 0.071 for SWNTs and 0.216 to 0.34 for MWNTs that demonstrate defect enhancement as a result of acid etching. Such enhancement in the extent of defects is consistently observed in the literature for oxidized CNTs [5, 40-43].

These defects formed during acid etching essentially break the hexagonal graphitic structure of CNTs and leave unbound carbon sites that are vulnerable to oxide group formation [40-41, 44]. Such dissociable oxide groups result in increased electrostatic interaction that facilitates dispersibility of the nano-reinforcement.

This observation is corroborated by the dispersion stability results obtained from TRDLS measurements (Figure 6). The hydrodynamic radius values with

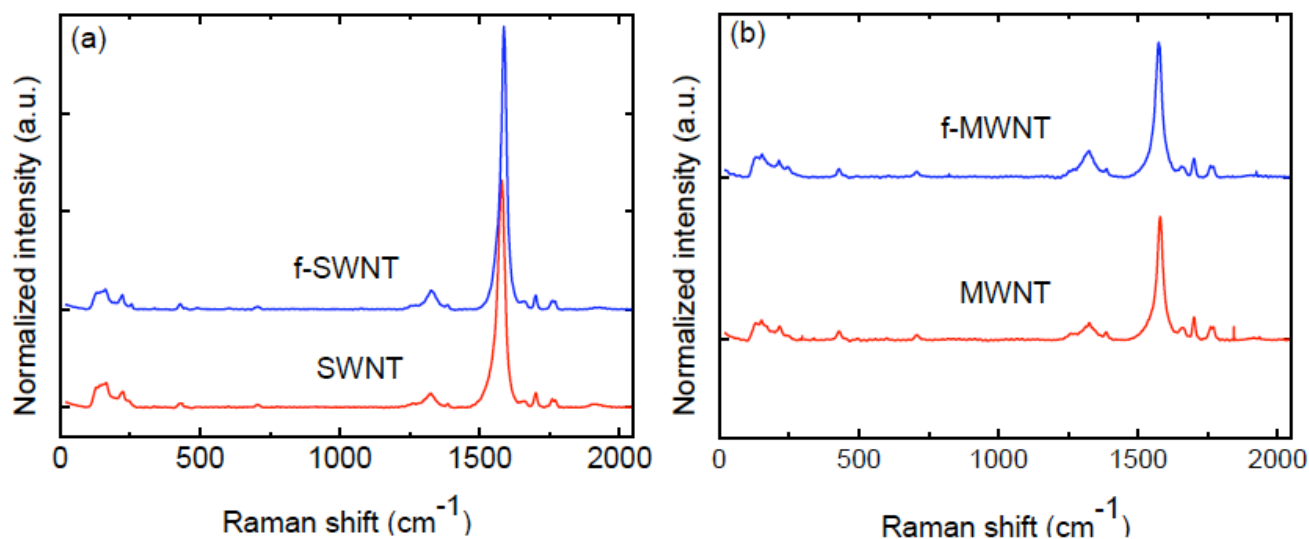


Figure 4: Raman spectra of pristine and functionalized (a) SWNTs and (b) MWNTs.

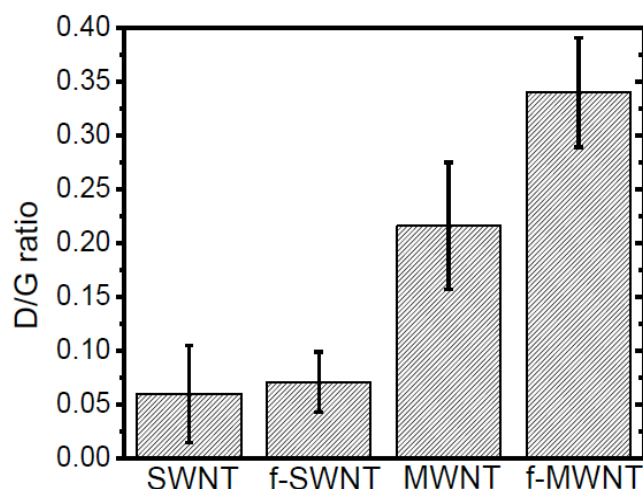


Figure 5: D/G ratios obtained from Raman spectroscopic measurements for pristine and functionalized SWNTs and MWNTs.

respect to time show uniform cluster size with little deviation from the average values of 146 ± 23 nm and 155 ± 11 nm for f-SWNT and f-MWNT aqueous suspensions, respectively. Such stable CNT cluster formation could be achieved due to the incorporation of functional groups *via* acid etching [46] as discussed through TEM and Raman characterization. The functional groups provide electrostatic interaction to the tubes and thus prevent aggregation and loss in stability, which is an inherent tendency of these all-carbon graphitic structures possessing high van der Waal's attraction [41]. Due to the interplay between repulsive electrostatic and attractive van der Waal's interaction, average cluster sizes observed in this study are consistent with those documented in the literature— 80-140 nm for SWNTs [41] and 150-200 nm for MWNTs [54-56].

Furthermore, the cluster size distributions of the CNTs are relatively uniform with narrow size distribution (Figure 7). These characterization results demonstrate effective functionalization and stable aqueous dispersion of SWNTs and MWNTs that were used to prepare the GNRC composite specimens.

3.2. TEM Images of GNRC Composites

Representative TEM micrographs from samples containing GNRC composite powder are shown in Figure 8. The sampling area for GNRC powder collection did not alter the TEM findings. Tubular structures, i.e., bundles of f-SWNTs (Figure 8a-b) and f-MWNTs (Figure 8c-d), are observed embedded within the cementitious matrix— appearing as crystalline features, likely to be the metal oxides of calcium-silicon-aluminum within the cement paste. Isolated and bundled tubes of tens and hundreds of nanometers are shown to bridge the cementitious matrix (Figures 8a and 8c). Figures 8b and 8d show higher magnification images that highlight the evidences of preferential association and embeddedness of the cementitious matrix with the f-CNTs—a visual demonstration of physical compatibility between the two materials obtained from samples of independent areas at the fracture surface. Moreover, distinctive SWNT and MWNT signatures are observed in the TEM micrographs as exemplified by the presence of single tubular layers in Figure 8b and multiple concentric layers in Figure 8d. Lengths of the CNTs as observed from TEM images are below 1 μm , in agreement with observations reported in the literature for functionalized CNTs (not embedded in composites) [45, 54]. As discussed earlier, such shortening has occurred due to acid etching of CNTs that oxidizes the ends with $-\text{COOH}$ termination [44, 46, 53]. Overall, the tubes

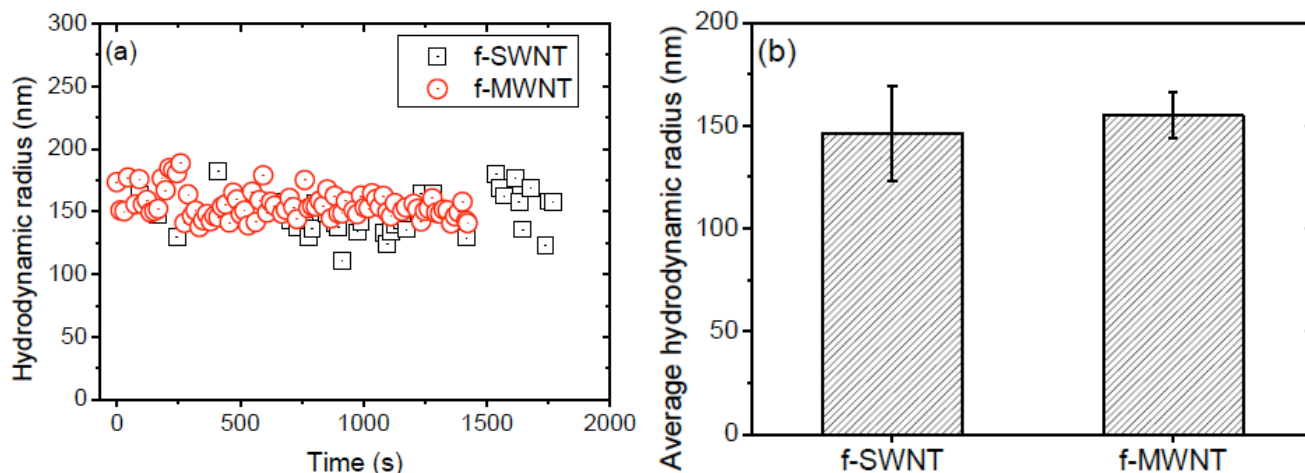


Figure 6: (a) Aqueous f-SWNT and f-MWNT profile and (b) average cluster size. Error bars represent one standard deviation.

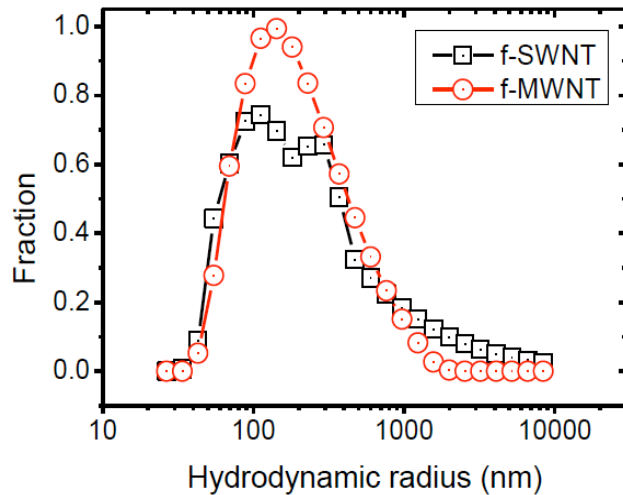


Figure 7: Representative particle size distribution of functionalized CNT dispersion.

observed in these TEMs, show substantial debundling for both f-SWNTs and f-MWNTs, which concurs with the earlier results of dispersion stability upon functionalization.

It is noted that the crystalline features of the cementitious matrix are often attached to the f-CNTs at the chemically active ends, produced through functionalization (Figure 8b). Literature findings for acid etching studies have shown tube breakage and creation of carboxylated sites, particularly at the ends of the CNTs [44, 57]—that can explain the preference of the cementitious matrix for the ends of CNTs. The demonstration of such preferential association of functionalized graphitic nano-reinforcement with the parent matrix is the first to-date visual representation at the interfacial nanoscale (sub-angstrom level resolution of TEM [58]) of physical compatibility between the materials in a GNRC composite. Based on this evidence, the colloidal technique for TEM imaging presented herein is a viable approach to investigate physical compatibility between graphitic nano-reinforcement and the cementitious matrix in GNRC composites—otherwise difficult to accomplish using surface imaging techniques (such as SEM) with one order of magnitude lower resolution [2-6, 11, 34-36, 59-61].

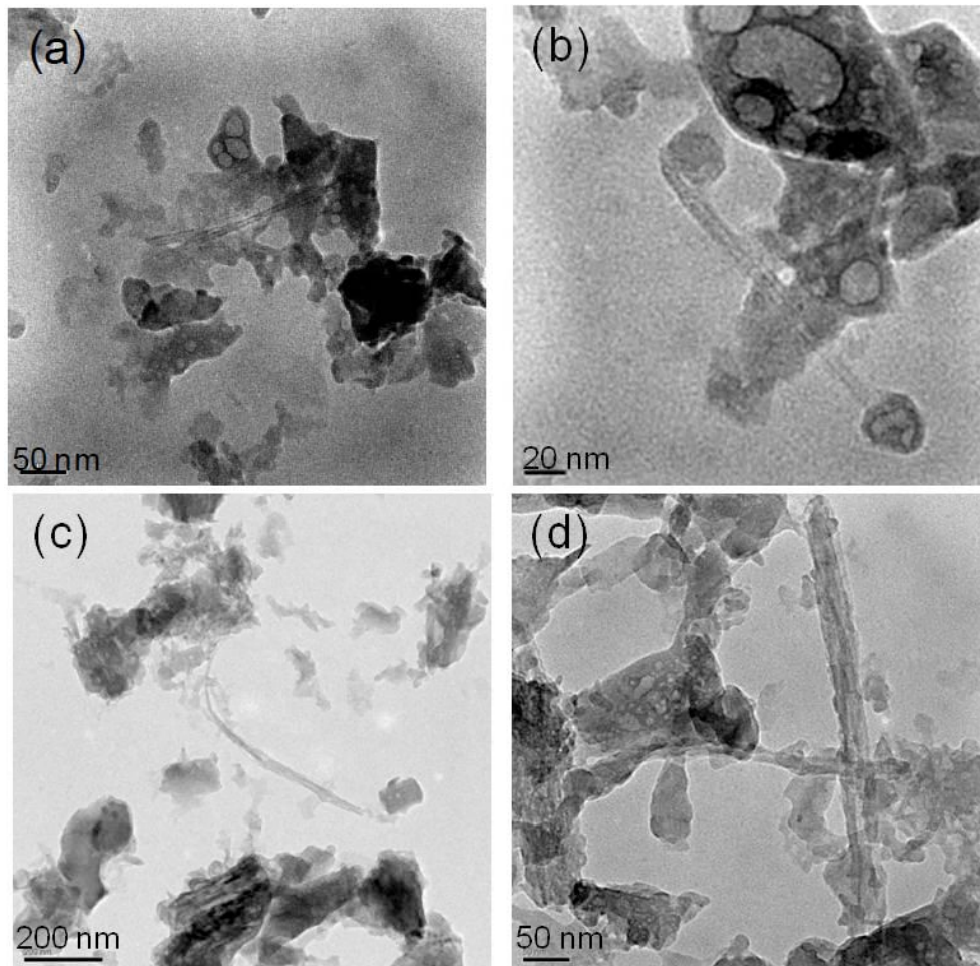


Figure 8: Representative TEM micrographs of GNRC composite powder with embedded (a-b) f-SWNTs and (c-d) f-MWNTs.

4. CONCLUSIONS

Uniform dispersion of graphitic nano-reinforcement and its chemical bond with cementitious matrices are key attributes to manufacture nano-reinforced cementitious composites with enhanced damage tolerance. This study reports effective functionalization of SWNTs and MWNTs using an acid etching technique. The f-SWNTs and f-MWNTs were used to prepare stable aqueous dispersions that were incorporated in the mix design for cementitious composite sample preparation. A novel colloidal approach was developed to image cementitious nanocomposites at the interfacial scale. The TEM imaging has produced high quality micrographs showing preferential association and embeddedness of the crystalline features of the cementitious matrix and f-SWNTs and f-MWNTs. The proposed methodology enables better characterization of physical compatibility between graphitic nano-reinforcement and cementitious material, and is a viable approach to advance the understanding of the nano-reinforcement-matrix interface chemistry.

ACKNOWLEDGEMENTS

The research presented in this paper has been funded through a University of South Carolina (USC) Promising Investigator Research Award (PIRA, PI F. Matta), the fourth and fifth authors' start-up resources, and the USC NanoCenter. Special thanks are extended to Ms. English Player, undergraduate assistant at USC, and Dr. Haijun Qian, Research Associate at the Clemson University Electron Microscope Facility.

REFERENCES

- [1] Sanchez F, Sobolev K. Nanotechnology in concrete - A review. *Constr Build Mater* 2010; 24(11): 2060-71. <http://dx.doi.org/10.1016/j.conbuildmat.2010.03.014>
- [2] Konsta-Gdoutos MS, Metaxa ZS, Shah SP. Multi-scale mechanical and fracture characteristics and early-age strain capacity of high performance carbon nanotube/cement nanocomposites. *Cem Concr Compos* 2010; 32(2): 110-15. <http://dx.doi.org/10.1016/j.cemconcomp.2009.10.007>
- [3] Tyson BM, Abu Al-Rub RK, Yazdanbakhsh A, Grasley Z. Carbon nanotubes and carbon nanofibers for enhancing the mechanical properties of nanocomposite cementitious materials. *J Mater Civ Eng* 2011; 23(7): 1028-35. [http://dx.doi.org/10.1061/\(ASCE\)MT.1943-5533.0000266](http://dx.doi.org/10.1061/(ASCE)MT.1943-5533.0000266)
- [4] Metaxa ZS, Konsta-Gdoutos MS, Shah SP. Mechanical properties and nanostructure of cement-based materials reinforced with carbon nanofibers and polyvinyl alcohol (PVA) microfibrils. *Am Concr Instit Special Publ* 2010; 270: 115-24.
- [5] Musso S, Tulliani JM, Ferro G, Tagliaferro A. Influence of carbon nanotubes structure on the mechanical behavior of cement composites. *Compos Sci Technol* 2009; 69(11-12): 1985-90. <http://dx.doi.org/10.1016/j.compscitech.2009.05.002>
- [6] Li GY, Wang PM, Zhao XH. Mechanical behavior and microstructure of cement composites incorporating surface-treated multi-walled carbon nanotubes. *Carbon* 2005; 43(6): 1239-45. <http://dx.doi.org/10.1016/j.carbon.2004.12.017>
- [7] Li GY, Wang PM, Zhao XH. Pressure-sensitive properties and microstructure of carbon nanotube reinforced cement composites. *Cem Concr Compos* 2007; 29(5): 377-82. <http://dx.doi.org/10.1016/j.cemconcomp.2006.12.011>
- [8] Gao D, Sturm M, Mo YL. Electrical resistance of carbon-nanofiber concrete (vol 18, 095039, 2010). *Smart Mater Struct* 2011; 20(4). <http://dx.doi.org/10.1088/0964-1726/20/4/049501>
- [9] Li KZ, Wang C, Li HJ, Li XT, Ouyang HB, Wei J. Effect of chemical vapor deposition treatment of carbon fibers on the reflectivity of carbon fiber-reinforced cement-based composites. *Compos Sci Technol* 2008; 68(5): 1105-14. <http://dx.doi.org/10.1016/j.compscitech.2007.08.003>
- [10] Xie XL, Mai YW, Zhou XP. Dispersion and alignment of carbon nanotubes in polymer matrix: A review. *Mater Sci Eng R-Rep* 2005; 49(4): 89-112. <http://dx.doi.org/10.1016/j.mser.2005.04.002>
- [11] Konsta-Gdoutos MS, Metaxa ZS, Shah SP. Highly dispersed carbon nanotube reinforced cement based materials. *Cem Concr Res* 2010; 40(7): 1052-59. <http://dx.doi.org/10.1016/j.cemconres.2010.02.015>
- [12] Richardson IG, Groves GW. Microstructure and microanalysis of hardened ordinary portland-cement pastes. *J Mater Sci* 1993; 28(1): 265-77. <http://dx.doi.org/10.1007/BF00349061>
- [13] Richardson IG, Groves GW. The structure of the calcium silicate hydrate phases present in hardened pastes of white Portland cement blast-furnace slag blends. *J Mater Sci* 1997; 32(18): 4793-802. <http://dx.doi.org/10.1023/A:1018639232570>
- [14] Aich N, Flora JRV, Saleh NB. Preparation and characterization of stable aqueous higher-order fullerenes. *Nanotechnology* 2012; 23(055705).
- [15] Rinzler AG, Liu J, Dai H, *et al.* Large-scale purification of single-wall carbon nanotubes: process, product, and characterization. *Appl Phys A-Mater Sci Process* 1998; 67(1): 29-37. <http://dx.doi.org/10.1007/s003390050734>
- [16] Wang ZL. Transmission electron microscopy of shape-controlled nanocrystals and their assemblies. *J Phys Chem B* 2000; 104(6): 1153-75. <http://dx.doi.org/10.1021/jp993593c>
- [17] Srikrishna K, Thomas G, Martinez R, Corral MP, Deaza S, Moya JS. Kaolinite mullite reaction-series - A TEM study. *J Mater Sci* 1990; 25(1B): 607-12. <http://dx.doi.org/10.1007/BF00714083>
- [18] Legros M, Gianola DS, Hemker KJ. In situ TEM observations of fast grain-boundary motion in stressed nanocrystalline aluminum films. *Acta Mater* 2008; 56(14): 3380-93. <http://dx.doi.org/10.1016/j.actamat.2008.03.032>
- [19] Akita T, Hiroki T, Tanaka S, *et al.* Analytical TEM observation of Au-Pd nanoparticles prepared by sonochemical method. *Catal Today* 2008; 131(1-4): 90-97. <http://dx.doi.org/10.1016/j.cattod.2007.10.033>
- [20] Engelmann HJ, Saage H, Zschech E. Application of analytical TEM for failure analysis of semiconductor device structures. *Microelectron Reliab* 2000; 40(8-10): 1747-51. [http://dx.doi.org/10.1016/S0026-2714\(00\)00107-4](http://dx.doi.org/10.1016/S0026-2714(00)00107-4)
- [21] Cabibbo M, Spigarelli S. A TEM quantitative evaluation of strengthening in an Mg-RE alloy reinforced with SiC. *Mater Charact* 2011; 62(10): 959-69. <http://dx.doi.org/10.1016/j.matchar.2011.04.011>

- [22] Daniel IM, Miyagawa H, Gdoutos EE, Luo JJ. Processing and characterization of epoxy/clay nanocomposites. *Exp Mech* 2003; 43(3): 348-54. <http://dx.doi.org/10.1007/BF02410534>
- [23] Mendez-Vilas A, Diaz J. Modern Research and Educational Topics in Microscopy. Microscopy Book Series, vol. 1 Mendez-Vilas, A. Diaz, J.: Formatex Research Center 2007. pp. 122-131.
- [24] Chen GX, Kim HS, Park BH, Yoon JS. Multi-walled carbon nanotubes reinforced nylon 6 composites. *Polymer* 2006; 47(13): 4760-67. <http://dx.doi.org/10.1016/j.polymer.2006.04.020>
- [25] Baji A, Mai YW, Wong SC, Abtahi M, Du XS. Mechanical behavior of self-assembled carbon nanotube reinforced nylon 6,6 fibers. *Compos Sci Technol* 2010; 70(9): 1401-409. <http://dx.doi.org/10.1016/j.compscitech.2010.04.020>
- [26] Broza G. Thermoplastic elastomers with multi-walled carbon nanotubes: Influence of dispersion methods on morphology. *Compos Sci Technol* 2010; 70(6): 1006-10. <http://dx.doi.org/10.1016/j.compscitech.2010.02.021>
- [27] Ye YP, Chen HB, Wu JS, Ye L. High impact strength epoxy nanocomposites with natural nanotubes. *Polymer* 2007; 48(21): 6426-33. <http://dx.doi.org/10.1016/j.polymer.2007.08.035>
- [28] Kornmann X, Lindberg H, Berglund LA. Synthesis of epoxy-clay nanocomposites: influence of the nature of the clay on structure. *Polymer* 2001; 42(4): 1303-10. [http://dx.doi.org/10.1016/S0032-3861\(00\)00346-3](http://dx.doi.org/10.1016/S0032-3861(00)00346-3)
- [29] Abdalla M, Dean D, Adibempe D, Nyairo E, Robinson P, Thompson G. The effect of interfacial chemistry on molecular mobility and morphology of multiwalled carbon nanotubes epoxy nanocomposite. *Polymer* 2007; 48(19): 5662-70. <http://dx.doi.org/10.1016/j.polymer.2007.06.073>
- [30] Li J, Malis T, Dionne S. Recent advances in FIB-TEM specimen preparation techniques. *Mater Charact* 2006; 57(1): 64-70. <http://dx.doi.org/10.1016/j.matchar.2005.12.007>
- [31] Walker JF, Reiner JC, Solenthaler C. Focused ion beam sample preparation for TEM. In: Cullis AG, StatonBevan AE, editors. *Microscopy of Semiconducting Materials* 1995; vol. 146: Bristol: Iop Publishing Ltd; 1995; pp. 629-634.
- [32] Wirth R. Focused Ion Beam (FIB) combined with SEM and TEM: Advanced analytical tools for studies of chemical composition, microstructure and crystal structure in geomaterials on a nanometre scale. *Chem Geol* 2009; 261(3-4): 217-29. <http://dx.doi.org/10.1016/j.chemgeo.2008.05.019>
- [33] Thangadurai P, Lumelsky Y, Silverstein MS, Kaplan WD. TEM specimen preparation of semiconductor-PMMA-metal interfaces. *Mater Charact* 2008; 59(11): 1623-29. <http://dx.doi.org/10.1016/j.matchar.2008.02.007>
- [34] Nochaiya T, Chaipanich A. Behavior of multi-walled carbon nanotubes on the porosity and microstructure of cement-based materials. *Appl Surf Sci* 2011; 257(6): 1941-45. <http://dx.doi.org/10.1016/j.apsusc.2010.09.030>
- [35] Metaxa ZS, Konsta-Gdoutos MS, Shah SP. Carbon nanofiber-reinforced cement-based materials. *Transp Res Record* 2010(2142): 114-18. <http://dx.doi.org/10.3141/2142-17>
- [36] Luo JL, Duan ZD, Li H. The influence of surfactants on the processing of multi-walled carbon nanotubes in reinforced cement matrix composites. *Phys Status Solidi A-Appl Mat* 2009; 206(12): 2783-90.
- [37] Grabar KC, Brown KR, Keating CD, Stranick SJ, Tang SL, Natan MJ. Nanoscale characterization of gold colloid monolayers: A comparison of four techniques. *Anal Chem* 1997; 69(3): 471-77. <http://dx.doi.org/10.1021/ac9605962>
- [38] Langley LA, Fairbrother DH. Effect of wet chemical treatments on the distribution of surface oxides on carbonaceous materials. *Carbon* 2007; 45(1): 47-54. <http://dx.doi.org/10.1016/j.carbon.2006.08.008>
- [39] Decker JE, Walker ARH, Bosnick K, *et al.* Sample preparation protocols for realization of reproducible characterization of single-wall carbon nanotubes. *Metrologia* 2009; 46(6): 682-92. <http://dx.doi.org/10.1088/0026-1394/46/6/011>
- [40] Saleh NB, Pfefferle LD, Elimelech M. Aggregation kinetics of multiwalled carbon nanotubes in aquatic systems: Measurements and environmental implications. *Environ Sci Technol* 2008; 42(21): 7963-69. <http://dx.doi.org/10.1021/es801251c>
- [41] Saleh NB, Pfefferle LD, Elimelech M. Influence of biomacromolecules and humic acid on the aggregation kinetics of single-walled carbon nanotubes. *Environ Sci Technol* 2010; 44(7): 2412-18. <http://dx.doi.org/10.1021/es903059t>
- [42] LeBlanc RJ, Chu W, Williams CT. Surface Raman characterization of cinchonidine-modified platinum in ethanol: effects of liquid-phase concentration and co-adsorbed hydrogen. *J Mol Catal A-Chem* 2004; 212(1-2): 277-89. <http://dx.doi.org/10.1016/j.molcata.2003.11.006>
- [43] Wepasnick KA, Smith BA, Schrote KE, Wilson HK, Diegelmann SR, Fairbrother DH. Surface and structural characterization of multi-walled carbon nanotubes following different oxidative treatments. *Carbon* 2011; 49(1): 24-36. <http://dx.doi.org/10.1016/j.carbon.2010.08.034>
- [44] Liu J, Rinzler AG, Dai HJ, *et al.* Fullerene pipes. *Science* 1998; 280(5367): 1253-56. <http://dx.doi.org/10.1126/science.280.5367.1253>
- [45] Hennrich F, Krupke R, Arnold K, *et al.* The mechanism of cavitation-induced scission of single-walled carbon nanotubes. *J Phys Chem B* 2007; 111(8): 1932-37. <http://dx.doi.org/10.1021/jp065262n>
- [46] Zhang J, Zou HL, Qing Q, *et al.* Effect of chemical oxidation on the structure of single-walled carbon nanotubes. *J Phys Chem B* 2003; 107(16): 3712-18. <http://dx.doi.org/10.1021/jp027500u>
- [47] Shelimov KB, Esenaliev RO, Rinzler AG, Huffman CB, Smalley RE. Purification of single-wall carbon nanotubes by ultrasonically assisted filtration. *Chem Phys Lett* 1998; 282(5-6): 429-34. [http://dx.doi.org/10.1016/S0009-2614\(97\)01265-7](http://dx.doi.org/10.1016/S0009-2614(97)01265-7)
- [48] Ziegler KJ, Gu ZN, Peng HQ, Flor EL, Hauge RH, Smalley RE. Controlled oxidative cutting of single-walled carbon nanotubes. *J Am Chem Soc* 2005; 127(5): 1541-47. <http://dx.doi.org/10.1021/ja044537e>
- [49] Giordani S, Colomer J-F, Cattaruzza F, *et al.* Multifunctional hybrid materials composed of [60]fullerene-based functionalized-single-walled carbon nanotubes. *Carbon* 2009; 47(3): 578-88. <http://dx.doi.org/10.1016/j.carbon.2008.10.036>
- [50] Moonosawmy KR, Kruse P. Ambiguity in the characterization of chemically modified single-walled carbon nanotubes: A Raman and ultraviolet-visible-near-infrared study. *J Phys Chem C* 2009; 113(13): 5133-40. <http://dx.doi.org/10.1021/jp810900b>
- [51] Hennrich F, Krupke R, Lebedkin S, *et al.* Raman spectroscopy of individual single-walled carbon nanotubes from various sources. *J Phys Chem B* 2005; 109(21): 10567-73. <http://dx.doi.org/10.1021/jp0441745>
- [52] Canete-Rosales P, Ortega V, Alvarez-Lueje A, *et al.* Influence of size and oxidative treatments of multi-walled carbon nanotubes on their electrocatalytic properties. *Electrochim Acta* 2012; 62: 163-71. <http://dx.doi.org/10.1016/j.electacta.2011.12.043>

- [53] Wang SR, Liang R, Wang B, Zhang C. Dispersion and thermal conductivity of carbon nanotube composites. *Carbon* 2009; 47(1): 53-57.
<http://dx.doi.org/10.1016/j.carbon.2008.08.024>
- [54] Smith B, Wepasnick K, Schrote KE, *et al.* Colloidal properties of aqueous suspensions of acid-treated, multi-walled carbon nanotubes. *Environ Sci Technol* 2009; 43(3): 819-25.
<http://dx.doi.org/10.1021/es802011e>
- [55] Smith B, Wepasnick K, Schrote KE, Cho HH, Ball WP, Fairbrother DH. Influence of surface oxides on the colloidal stability of multi-walled carbon nanotubes: A structure-property relationship. *Langmuir* 2009; 25(17): 9767-76.
<http://dx.doi.org/10.1021/la901128k>
- [56] Brady-Estevez AS, Schnoor MH, Vecitis CD, Saleh NB, Ehmelech M. Multiwalled carbon nanotube filter: Improving viral removal at low pressure. *Langmuir* 2010; 26(18): 14975-82.
<http://dx.doi.org/10.1021/la102783v>
- [57] Marshall MW, Popa-Nita S, Shapter JG. Measurement of functionalised carbon nanotube carboxylic acid groups using a simple chemical process. *Carbon* 2006; 44(7): 1137-41.
<http://dx.doi.org/10.1016/j.carbon.2005.11.010>
- [58] O'Keefe MA, Hetherington CJD, Wang YC, *et al.* Sub-Angstrom high-resolution transmission electron microscopy at 300 keV. *Ultramicroscopy* 2001; 89(4): 215-41.
[http://dx.doi.org/10.1016/S0304-3991\(01\)00094-8](http://dx.doi.org/10.1016/S0304-3991(01)00094-8)
- [59] Chaipanich A, Nochaiya T, Wongkeo W, Torkittikul P. Compressive strength and microstructure of carbon nanotubes-fly ash cement composites. *Mater Sci Eng A-Struct Mater Prop Microstruct Process* 2010; 527(4-5): 1063-67.
<http://dx.doi.org/10.1016/j.msea.2009.09.039>
- [60] Mojumdar SC, Raki L. Synthesis, thermal and structural characterization of nanocomposites for potential applications in construction. *J Therm Anal Calorim* 2006; 86(3): 651-57.
<http://dx.doi.org/10.1007/s10973-006-7720-1>
- [61] Han BG, Yu X, Kwon E. A self-sensing carbon nanotube/cement composite for traffic monitoring. *Nanotechnology* 2009; 20(44).
<http://dx.doi.org/10.1088/0957-4484/20/44/445501>

Received on 30-08-2012

Accepted on 22-09-2012

Published on 31-10-2012

[DOI: http://dx.doi.org/10.6000/1929-5995.2012.01.01.3](http://dx.doi.org/10.6000/1929-5995.2012.01.01.3)